PAPER

Check for updates

On the interaction of softwood hemicellulose with cellulose surfaces in relation to molecular structure and physicochemical properties of hemicellulose†

Polina Naidjonoka, [iD] *[a] Monica Arcos Hernandez,[b] Gunnar K. Pálsson,[cd] Frank Heinrich,[ef] Henrik Stålbrand [iD] *[g] and Tommy Nylander [iD] *[ahi]

The substantial part of the water-soluble hemicellulose fraction, obtained when processing cellulose to produce paper and other products, has so far been discarded. The aim of this work is to reveal the interfacial properties of softwood hemicellulose (galactoglucomannan, GGM) in relation to their molecular and solution structure. In this study the sugar composition of GGM was characterised by chemical analysis as well as 1D and 2D NMR spectroscopy. Previously it has been demonstrated that hemicellulose has high affinity towards cellulose and has the ability to alter the properties of cellulose based products. This study is focused on the interactions between hemicellulose and the cellulose surface. Therefore, adsorption to hydrophobized silica and cellulose surfaces of two softwood hemicellulose samples and structurally similar seed hemicelluloses (galactomannans, GMs) was studied with ellipsometry, QCM-D and neutron reflectometry. Aqueous solutions of all samples were characterized with light scattering to determine how the degree of side-group substitution and molecular weight affect the conformation and aggregation of these polymers in the bulk. In addition, hemicellulose samples were studied with SAXS to investigate backbone flexibility. Light scattering results indicated that GM polymers form globular particles while GGMs were found to form rod-like aggregates in the solution. The polysaccharides exhibit higher adsorption to cellulose than on hydrophobic surfaces. A clear correlation between the increase in molecular weight of polysaccharides and increasing adsorbed amount on cellulose was observed, while the adsorbed amount on the hydrophobic surface was fairly independent of the molecular weight. The obtained layer thickness was compared with bulk scattering data and the results indicated flat conformation of the polysaccharides on the surface.

Introduction

The interactions between hemicellulose and another major wood polysaccharide, cellulose, are of key importance for the organization and structure of the plant cell walls as well as for a range of applications. The major components of softwood hemicellulose are galactoglucomannans (GGM). Their content varies both in different parts of the tree, as well as between plant species with GGM, reaching up to 20% w/w of dry wood.[1–4] Today a significant part of the softwood GGM is discarded together with the waste stream during processes like thermo-mechanical pulp production.[5] However, it is now possible to recover this highly valuable polymer from such waste streams.[6–8] While other mannan-based polysaccharides like Locust bean gum (LBG) and Guar gum (GG) are used in the industry, mostly in food related applications,[9–12] GGMs from softwood are not yet fully exploited in spite of the large amount produced during pulp processing. However, numerous potential applications have been suggested and tested for GGMs in therapeutic reagents,[13] as a raw material for biodegradable films[14–16] and novel anticoagulants.[17] Therefore, this study focuses on the interfacial interactions between cellulose and softwood hemicellulose and how it relates to the aggregation and molecular architecture in comparison to other mannan-based polysaccharides.

[a] *Physical Chemistry, Department of Chemistry, Lund University, Lund, Sweden. E-mail: polina.naidjonoka@fkem1.lu.se, tommy.nylander@fkem1.lu.se*
[b] *Polymer & Materials Chemistry, Department of Chemistry, Lund University, Lund, Sweden*
[c] *Department of Physics & Astronomy, Uppsala University, Uppsala, Sweden*
[d] *Institut Laue Langevin, Grenoble, France*
[e] *Department of Physics, Carnegie Mellon University, Pittsburgh, PA, USA*
[f] *NIST Center for Neutron Research, Gaithersburg, MD, USA*
[g] *Biochemistry and Structural Biology, Department of Chemistry, Lund University, Lund, Sweden. E-mail: henrik.stalbrand@biochemistry.lu.se*
[h] *NanoLund, Lund University, Lund, Sweden*
[i] *Lund Institute of Advanced Neutron and X-ray Science LINXS, Lund, Sweden*
† Electronic supplementary information (ESI) available. See DOI: 10.1039/d0sm00264j

Hemicellulose has a large number of side groups and their role for interaction with cellulose and to what extent they prevent the polysaccharide to assemble into larger aggregates is not clear. GGMs consist of a β-(1→4)-ᴅ-mannopyranose backbone that is partially interrupted by β-(1→4)-ᴅ-gluco-pyranose units.[1,18,19] The backbone carries side-groups of α-(1→6)-ᴅ-galactopyranose and acetyl side groups.[18] The degree of side-group substitution may vary between sources and preparations. Galactoglucomannans are mainly present in the secondary cell walls of conifer plants, however, small amounts are also found in dicot cell walls.[3] Locust bean gum is produced in the seed endosperm of the carob tree *Ceratonia silique L.* and Guar gum in the seed of *Cyamopsis tetragonoloba*. Both LBG and GG contain only β-(1→4)-mannopyranose in the backbone and galactopyranose side-groups attached *via* α-(1→6) linkages.

In wood, cellulose forms microfibrils that are well organized with chains of hemicellulose located either on the surface of or in between the fibrils.[20] The nature of the binding of hemicellulose is still under debate, however, it is believed that the polysaccharides interact with each other *via* hydrogen bonding.[21,22] Benselfelt *et al.*[23] showed that the adsorption of xyloglucan, the main hemicellulose in primary plant cell walls, onto cellulose surfaces is an entropy-driven process. An increase in entropy is caused by the release of water molecules from the cellulose layer as hemicellulose is adsorbed.

Several approaches have been used to reveal the nature of the interaction between cellulose and hemicellulose. Hayashi *et al.*[20,24] studied the influence of the polymerization degree on the adsorption of xyloglucan on dispersed cellulose. They demonstrated that xyloglucans adsorb to the microfibrils of cellulose as a monolayer with highly branched parts extending into solution. The adsorption per weight unit was found to be larger on microcrystalline cellulose compared to amorphous cellulose. Similar results were obtained by Vincken *et al.*[22] where xyloglucan was found to bind more efficiently to microcrystalline cellulose Avicel than to cellulose from cotton linters. Avicel has a 10 times smaller exposed surface-to-weight ratio than bacterial cellulose, but the per-area-adsorption of the polymeric xyloglucans is similar.[25] Uhlin *et al.*[26] used *Acetobacter xylinum* as a model system to produce cellulose in the presence of carboxymethyl cellulose (CMC), xylan, xyloglucan and ivory nut mannan. These polysaccharides were shown to affect cellulose structure in different ways. Xyloglucans and xylans showed the largest effect on the aggregation of cellulose due to a similarity in the backbone unit conformation with cellulose. Cellulose produced in the presence of mannans and CMC was found to have a very similar aggregation pattern but with a lower degree of cellulose crystallinity in comparison to a control grown without the polysaccharides. The charge of hemicellulose was found to be more crucial than the molecular weight for the adsorption to nanofibrillated cellulose (NFC). The adsorbed amount of Guar gum before and after hydrolysis showed comparable results in similar conditions. The adsorption of the anionic CMC showed strong dependence on the pH of the buffer, with irreversible adsorption at low pH but not at pH 8 where the carboxylic groups of both CMC and cellulose are deprotonated.[27,28]

The sorption of glucomannans to cellulose is affected by the presence of side groups that prevent a close contact of the polysaccharide with the cellulose fibre surface. In addition, by removing the side groups, solubility of the chains of the polysaccharides chain decreases[29–31] and promotes binding to a surface. Deacetylation generates new hydroxyl groups that can take part in hydrogen bonding[5,32] and at least 15 unsubstituted xylosyl units are required for adsorption.[25]

It is clear that the increasing use of hemicelluloses requires knowledge on how their molecular structure affect bulk solution behaviour and the adsorption to different types of surfaces. Here we compared the results of two types of GGMs, with different molecular weight and degree of side-group substitution, with those from seed hemicelluloses (LBG and GG). The LBG and GG samples are commonly used in industrial applications. Solution behaviour of the polysaccharides was characterized with light and small angle X-ray scattering, which gave information on the size, shape and stiffness, as well as the aggregation state of the polysaccharides. The knowledge gained from the polysaccharide molecular structure, conformation and aggregation was related to the results from adsorption studies on two relevant surfaces for applications, *i.e.* hydrophobic and spin-coated cellulose films. The combination of *in situ* ellipsometry, quartz crystal microbalance with dissipation (QCM-D) and neutron reflectometry (NR) allowed us not only to quantify the adsorption in terms of surface excess and adsorption kinetics, but by comparing the adsorption onto a cellulose surface with that on a hydrophobic surface we were able to gain insight into the nature of the surface interactions of hemicellulose.

Experimental

Materials

Galactomannans. Galactomannan polysaccharides Guar gum and Locust bean gum were obtained from Megazyme International (Bray, Ireland).

Preparation of GGM. Two types of GGM-enriched preparations originating from spruce were used in the study. The first one (TMP-GGM) was obtained from the process water from termomechanical pulp processing and GGM was purified using ultrafiltration and four rounds of diafiltration as described in detail by Andersson *et al.*[6] To prepare SP-GGM, steam extraction of GGM from spruce chips in 0.025% NaOH was performed at 190 °C for 5 minutes according to Lundqvist *et al.*[2] The liquid phase was then filtered and GGM purified by size-exclusion chromatography (SEC) with recovery of the "F1-fraction" as described by Palm and Zacchi.[33] The GGM preparations were freeze-dried and stored under dry conditions at room temperature.

Chemical analysis of GGM samples. The GGM preparations were analysed for sugar monomer composition, acetyl content and weight-average molecular weight (M_w) as described by Lundqvist *et al.*[2] The sugar monomer composition was determined after hydrolysis in an autoclave at 120 °C in 0.25 M sulphuric acid. Monomer sugar analysis (mannose, galactose, glucose, xylose, arabinose) was performed using high-performance liquid

chromatography with pulsed amperometric detection (HPAEC-PAD), using a Carbo Pac Pa10 guard and analytical column (Dionex/Thermofischer Scientific). The acetyl content was analysed after treatment in 1% NaOH for 12 h at room temperature and quantification of acetic acid by high-performance liquid chromatography (HPLC) using an Aminex HPX-87H (BIO-RAD) column and refractive-index (RI) detection. M_w was estimated using SEC (RI-detection) with water as eluent and using GGM mass-standards analysed by matrix-assisted laser ionization/desorption time-of-light (MALDI-TOF).[2] The lignin content was estimated by measuring the absorbance at 280 nm of water-dissolved samples and using an extinction coefficient of 17.8 L g^{-1} cm^{-1} (for milled wood lignin) previously suggested applicable for water soluble spruce lignin from mechanical pulp processing.[34]

1D and 2D NMR spectroscopy. Dried samples were dissolved in 0.6 mL of 99.9% deuterium oxide (Sigma Aldrich Co., MO, USA) to a concentration of 10 mg mL^{-1}. ^{1}H and ^{13}C spectra as well as heteronuclear single quantum coherence (HSQC) NMR spectra were recorded at 25 °C, 12 or 70 °C on a Bruker Avance III spectrometer (Bruker, Billerica, MA, USA) at 500.17 MHz for ^{1}H and at 125.77 MHz for ^{13}C. Chemical shifts were referenced to the C-1 signal of glucopyranose (103.548 ppm) and the H-2 signal of the 2-O-acetylated mannopyranose (5.423 ppm).[19,35] The chosen temperatures for spectra acquisition were different to room temperature in order to induce a shift of the residual internal solvent (HDO) to reveal or improve the resolution of the anomeric signals arising from the sugar units. HSQC was acquired at 25 °C using the same method as described in Al-Rudainy et al.[8] with minor adjustment for specific samples (adjustment of SR, sweep width and O 1p and O 2p parameters). Data was processed with Topspin (Bruker) or MestreNova (Mestrelab Research). Baseline and phase correction were applied in both directions. ^{1}H NMR was used for quantification as described in Rosengren et al. using an external standard[36] as well as using the module ERETIC 2 for quantification which is based on PULCON,[37] an internal standard method which correlates the absolute intensities of two different spectra (Topspin, Bruker).

Microcrystalline cellulose. Microcrystalline cellulose (Avicel PH101, Sigma-Aldrich, Sweden) with an average particle size of 50 μm, N,N-dimethylacetamide (DMAc), lithium chloride (99.0% LiCl) and dimethyloctylchlorosilane (DMOCS, 97%) were purchased from Sigma-Aldrich, Sweden. LiCl$_2$ was dried at 200 °C overnight and used immediately. Purified water (18 MΩ cm) was obtained by passing deionized water through a Milli-Q® Water Purification system (MerckMillipore, Darmstadt, Germany) was used for the preparation of all solutions. All other solvents and reagents were of analytical grade and were used as received.

Sample preparation. GG and LBG solutions (5 mg mL^{-1}) in sodium citrate buffer (0.05 M, pH 5.9) were prepared by adding 1.0 g of powder to 180 mL of buffer. The mixture was then homogenized with Heidolph DIAX 900 homogenizer (Heidolph Instruments GmbH, Schwabach, Germany) (using 5 pulses at a setting 1) at 80 °C and heated to the boiling point under agitation. The obtained viscous solution was cooled down to a room temperature while continuing agitation overnight at 4 °C. The solution was then centrifuged (5338 × g, 20 min) to remove impurities and diluted with the buffer to 200 mL. Aliquots of clear solution were stored at −20 °C until further use. After thawing, the solution was vigorously stirred.

LvLBG was dissolved by wetting 1 g of powder with 2 mL of 95% ethanol followed by the addition of 90 mL sodium citrate buffer (0.05 M, pH 5.9) and stirring overnight at 4 °C. Thereafter, the solution was heated to 120 °C in a beaker covered with aluminium foil and under vigorous stirring with an IKA RCT basic magnetic stirrer. Stirring continued without heating for approximately 20 min until complete dissolution. The solution was then centrifuged (5338 × g, 10 min) to remove impurities and diluted with buffer to a final volume of 100 mL.[38]

GGM samples (10 mg mL^{-1}) were dissolved directly in 0.05 M citrate buffer and stored at +4 °C for maximum 1 week until further use. Cellulose solutions were prepared according to Sczech et al.[39] Microcrystalline cellulose powder (1 g) was first left to swell for 1 h in 10 mL of deionized water at 40 °C. Excess of water was then removed from the hydrated cellulose by centrifugation (2616 × g, 15 min). This was followed by an exchange with 10 mL of methanol, after which the mixture was incubated during stirring for 45 min, followed by centrifugation at 2616 × g for 15 min to remove the excess of the solvent. The same procedure was repeated once more with methanol and then twice with the anhydrous DMAc. After the last incubation, the mixture was centrifuged, and the cellulose pellet was then dissolved in 100 mL of 7% (w/v) LiCl/DMAc solution under stirring at room temperature for 15 h. The cellulose solution was then placed at 4 °C under stirring until the cellulose was completely dissolved.

Substrate preparation. Substrates used for the ellipsometry measurements were polished silicon wafers (p-type, boron-doped, resistivity of 1–20 Ω cm) which were obtained from SWI (Semiconductor Wafer, Inc., Taiwan). The wafers were thermally oxidized at 920 °C in an oxygen atmosphere to yield a 300 Å thick SiO$_2$ layer.

Silicon wafers were cut into 2 × 1 cm pieces and cleaned according to Chang et al.[40] Silica substrates were placed in a base mixture of 25% NH$_4$OH, 30% H$_2$O$_2$, and H$_2$O (1/1/5 by volume) at 80 °C for 5 min, rinsed with deionized water, and cleaned in an acid mixture of 32% HCl, 30% H$_2$O$_2$ and H$_2$O (1/1/5 by volume) at 80 °C for 5 min. The substrates were thoroughly rinsed with water and ethanol, and stored in ethanol (99.7%) until further use.

Polished silicon substrates (Siltronix, Archamps-France) of 5 × 5 × 1.5 cm^3 capped with a silicon oxide layer were used for Neutron Reflectometry (NR) measurements. Surfaces were cleaned as described above.

The substrates used for Quartz Crystal Microbalance with Dissipation (QCM-D, Q-Sense Analyzer, Biolin Scientific, Gothenburg, Sweden) measurements were quartz crystals (Q-Sense QSX 303) coated with gold and a top layer of SiO$_2$ exposed to the solution. The fundamental frequency of the

crystals was 4.95 MHz. The quartz QCM crystals were cleaned for 5 min in 2% (v/v) Hellmanex III® while sonicating and rinsed with water and 99.7% ethanol.

Hydrophobized silica substrates were prepared by first treating cleaned silica surfaces in an air plasma for 5 min at 0.02 mbar using a plasma cleaner (Harrick Scientific Corp, model PDC-3XG, New York, USA). The samples were then immediately placed in a desiccator under vacuum with 1 mL of DMOCS overnight. The hydrophobized silicon wafers were subsequently sonicated for 20 min in tetrahydrofuran and ethanol and stored in ethanol. Substrates were carefully rinsed with ethanol and water, and dried with nitrogen gas before each experiment.

Cellulose surfaces were prepared by spin-coating a few drops of clear cellulose solution on the silica surface (spin coater module LabSpin6/8, SUSS MicroTec SE, Germany) at 6000 rpm for 60 s. The spin-coated wafers were annealed at 100 °C for 10 min, cooled down to room temperature, placed into deionized water for 20 min, dried in a nitrogen flow and heated at 150 °C for 15 min. The cellulose covered substrates were used immediately. The cellulose film thickness was roughly 40 nm for all the substrates used for the ellipsometry measurements.

Dynamic and static light scattering (DLS and SLS). Both static and dynamic light scattering experiments were performed on an ALV/DLS/SLS-5022F, CGH-8F-based compact goniometer system (ALV-GmbH, Langen, Germany) with a 22 mW He–Ne-laser (632.8 nm) light source. The instrument was equipped with an automatic attenuator, controlled *via* software. The sample holder consists of a cell housing filled with a refractive index matched liquid (*cis*-decahydronaphtalene) in which the cuvette was placed.

Light scattering data from GGM samples were recorded at a concentration of 1.5 mg mL^{-1} and from galactomannans at 3 mg mL^{-1} dissolved in 0.05 M citrate buffer (pH 5.9). All samples were filtered with a 0.45 μm-pore-size filter and transferred to clean borosilicate NMR tubes prior to the measurements. For SLS, angles from 40° to 140° were used with a step size of 2° for 6 s. The intensity autocorrelation functions were obtained for angles from 60° to 130° with steps of 10° for at least 300 s. All the measurements were performed at 25 °C.

For the static light scattering, the obtained scattering intensity $I(q)$ was corrected for background scattering ($\Delta I(q)$) and brought to an absolute scale according to eqn (1)[41]

$$I(q) = \frac{\Delta I(q)}{I_{ref}(q)} \left(\frac{n}{n_{ref}}\right)^2 RR_{ref} \tag{1}$$

where n is the refractive index of the solution, and $I_{ref}(q)$, n_{ref} and RR_{ref} are the scattered intensity, refractive index, and Rayleigh ratio, of the reference (toluene), respectively. q is the magnitude of the scattering vector:

$$q = \frac{4\pi n}{\lambda_0} \sin\left(\frac{\theta}{2}\right) \tag{2}$$

where λ_0 is the laser wavelength, n is the refractive index of the solution and θ is the scattering angle. The radius of gyration R_G was determined using Zimm plots.

The decay rate (Γ) was obtained from the second order cumulative expansion,[42] which was plotted at different scattering vectors. The slope of such a plot gives the translational diffusion coefficient D. The hydrodynamic radius R_H was calculated according to the Stokes–Einstein equation:

$$D = \frac{k_B T}{6\pi\eta R_H} \tag{3}$$

where k_B is the Boltzmann constant, T is the temperature and η is the solvent viscosity.

Small-angle X-ray scattering (SAXS). SAXS measurements were performed at the SWING beamline at the SOLEIL Synchrotron (Gif-sur-Yvette, France). The instrument was equipped with an Eiger 4M (Dectris) detector. The X-ray wavelength was 1.54 Å^{-1}. Small-Angle X-ray Scattering curves were recorded for SP and TMP samples in 0.05 M citrate buffer (pH 5.9) at three different concentrations: 5 mg mL^{-1}, 10 mg mL^{-1} and 20 mg mL^{-1}. A flow capillary set up was used for all the samples. Buffer was flushed through the capillary and measured before and after each sample to ensure a clean capillary and to account for fluctuations in the beam intensity. The data were collected for two different q-ranges (0.0049–0.44 Å^{-1} and 0.0027–0.24 Å^{-1}) with an exposure time of 500 ms. Collected scattering curves were reduced and stitched together using the Foxtrot Software (https://www.synchrotron-soleil.fr/en/beam lines/swing). The reduced data was evaluated with SasView.[43] The scattering curves for both samples were fitted to the Unified Exponential/Power-law model developed by Beaucage[44–46] that describes fractal-like behavior of polymers in solution.

Cryogenic-transmission electron microscopy (Cryo-TEM). Samples for Cryo-TEM at a concentration of 1.5 mg mL^{-1} were filtered through a 0.45 μm-pore-size filter. A 4 μL-sample drop was placed on a lacey carbon coated formvar grid (Ted Pella Inc., Redding, CA, USA) and gently blotted with a filter paper to create a thin film. The grid was then prepared for imaging using an automatic plunge-freezer system (Leica Em GP, Leica Microsystems, Wetzlar, Germany) with the environmental chamber operated at 25 °C and 90% relative humidity to prevent evaporation from the specimen. The vitrification of the specimen was performed by rapid plunging of the grid into liquid ethane (−183 °C). Thereafter, samples were stored in liquid nitrogen (−196 °C) and transferred into the microscope using a cryo transfer tomography holder (Fischione, Model 2550, E. A. Fischione Instruments, Inc., Corporate Circle Export, PA, USA). The grids were examined with a Jeol JEM-2200FS transmission electron microscope (JEOL, Tokyo, Japan) equipped with a field-emission electron source, a cryo-pole piece in the objective lens and an in-column energy filter (omega filter). Zero-loss images were recorded under low-dose conditions at an acceleration voltage of 200 kV on a bottom-mounted TemCam-F416 camera (TVIPS-Tietz Video and Image Processing Systems GmbH, Gauting, Germany) using SerialEM.

Atomic force microscopy (AFM). AFM was performed with a Park XE-100 (Park Systems Corp., Suwon, Korea) in a non-contact mode. Samples were probed in dry state under ambient conditions. A silicon cantilever with a 42 N m^{-1} spring constant

and 330 kHz resonance frequency was used. The image analysis was done with the XEI software (Park Systems Corp., Suwon, Korea).

Ellipsometry. The main technique used to study the interfacial behavior of GGM is ellipsometry with complimentary information obtained by QCM-D and neutron reflectometry. The adsorption of hemicellulose to cellulose and hydrophobic surfaces were measured *in situ* using null ellipsometry as described previously.[47] This method is based on the changes in the polarization state when elliptically polarized light is reflected from a surface. A Rudolph Research ellipsometer (type 43603-200E) equipped with a xenon arc lamp light source was used for the adsorption study. All measurements were performed at 4015 Å wavelength and an incidence angle of 68.00°. The silicon substrates were placed inside a trapezoid cuvette with volume of 5 mL that was held at 25 °C.

The optical properties of the silicon substrates were characterized before each experiment in two different media, air and aqueous buffer. To minimize the effect caused by imperfections of the optical components, the average positions of polarizer and analyzer in four zones were used to calculate the ellipsometric angles, ψ and Δ. Here, ψ represents the change in the relative amplitude and Δ, the phase shift of polarized light upon reflection at the interface. From the ellipsometric angles, the refractive index and layer thickness of the adsorbed layer were determined using a three or four layer optical model.[47] The adsorbed amount Γ was calculated using the de Feijter equation[48]

$$\Gamma = \frac{(n_f - n_0)d_f}{dn/dc} \tag{4}$$

where n_0, n_f, d_f and dn/dc are the refractive index of the medium, the mean refractive index of the adsorbed layer, the optical thickness of the layer and the specific refractive index increment, respectively. The dn/dc values used for the calculations and the references are summarized in Table 1.

After the characterization of the bare surface, a polysaccharide solution was added to the ellipsometry cuvette to a final concentration of 0.02 mg mL^{-1}. For the experiments with cellulose surfaces, pre-characterized silicon wafers were spin-coated with the cellulose solution before the addition of the sample.

As soon as the system reached an equilibrium, the cuvette was flushed with fresh buffer solution to remove the polysaccharide solution. This allowed to estimate the extent of reversible mannan binding to the substrate.

Quartz crystal microbalance with dissipation (QCM-D). QCM-D is an acoustic technique that measures changes in the resonance frequency of a quartz crystal due to adsorption or deposition of material on its surface. The change in

frequency is recorded as a function of time while a substance is adsorbing to the substrate. The dissipation energy is measured by monitoring the decay of the signal amplitude when switching off the potential across the crystal and yields viscoelastic properties of the surface layer.[52] A QSense E4 system with four flow cells (Biolin Scientific, Gothenburg, Sweden) was used.

Hydrophobized crystals were placed in the flow cell and ethanol was passed through the system with peristaltic pump (Ismatec IPC-N 4, Zürich, Switzerland), followed by purging with 0.05 M citrate buffer (pH 5.9). The crystals were left to stabilize in the buffer for at least 30 min. The fundamental frequencies and dissipation energies for each overtone were determined before samples were injected at 150 μL min^{-1} at a concentration of 0.02 mg mL^{-1}. All measurements were performed at 25 °C. The obtained data was treated and fitted with a Voigt viscoelastic model[53] using Dfind software (QSense, Biolin Scientific).

Neutron reflectometry (NR). Neutron reflectometry is a technique, where a neutron beam is directed towards a surface and the intensity of the reflected radiation as a function of scattering vector q (see eqn (5)) is measured.

$$q = \frac{4\pi}{\lambda_0} \sin(\theta_{in}) \tag{5}$$

where λ_0 is the neutron wavelength and θ_{in} is the angle of incidence.

Here we used specular NR, *i.e.* the angle of reflection is equal to the incident beam angle.[54] Measurements were performed at NIST Center For Neutron Research (NCNR, Gaithersburg, MD) on the NGD-MAGIK reflectometer over a q-range of 0.005–0.2 Å^{-1}.[55]

Adsorption of TMP GGM was studied with NR on a hydrophobic surface. TMP was dissolved in deuterated 0.05 M citrate buffer (pH 5.9) at a concentration of 0.2 mg mL^{-1}. First, the specular reflectivity of the bare surface immersed in deuterated (D$_2$O) and protonated (H$_2$O) buffer was measured *versus* q. The sample in D$_2$O buffer was then injected and left for 1 hour to adsorb. Thereafter, two NR curves were measured after rinsing with D$_2$O and H$_2$O-based buffers, respectively. The raw data was reduced with the online data reduction service *reductus*.[56] The reduced data was evaluated with the Motofit software, which uses the Abeles matrix method to calculate the reflectivity from a stratified interfaces.[57,58] The best fit was obtained applying 4 layers as follows: Si–SiO$_2$, hydrophobic layer, the transition layer containing acetyl groups of GGM interconnected with the hydrophobic layer and the top layer mainly consisting of the GGM sugar units. The layer thickness, roughness, solvent penetration and Scattering length density (SLD) were found for each layer by simultaneously fitting the model to the data from H$_2$O and D$_2$O contrasts. Attempt was also made to measure the interaction between GGM and the cellulose layer using neutron reflectometry. However, the poor SLD contrast between GGM and cellulose made modelling uncertain and we therefore prefer not to discuss these data. We are at the moment working on neutron reflectometry study where we use deuterated cellulose to enhance the SLD contrast.

Table 1 dn/dc values of polysaccharides

Polysaccharide	dn/dc [mL g^{-1}]	Ref.
LBG, LvLBG, GG	0.135	49
GGMs	0.148	50
Cellulose	0.131	51

Results and discussion

Chemical analysis

The results from the chemical analysis are summarized in Table 2. Assuming polymeric mannose, galactose, glucose and acetyl content comprise acetylated GGM (AcGGM), this component accounted for 77% and 83% of the dry-weight for the TMP-GGM and SP-GGM preparations, respectively. The SP-GGM preparation contained arabinoxylan, estimated from the acid released xylose and arabinose as described above (Table 2). No detectable arabinoxylan was present in TMP-GGM. The lignin content was estimated to be 3.0% (TMP-GGM) and 3.3% (SP-GGM) of the dry weight, based on simple UV light absorption measurements.

1D and 2D NMR spectroscopy

Expansions of the 2D-NMR data in the anomeric region of SP and TMP preparations are shown in Fig. 1. The proton NMR resonances in the anomeric region were assigned based on HSQC and confirmed by comparison with literature.[18,19,59–61] The spectra recorded for both samples are similar confirming the similarity of the two samples. Hence, the SP is used as a template to describe assignments of the peaks. Table 3 shows the assignation in the anomeric area for SP using HSQC (the corresponding data for TMP are shown in the ESI†).

Spectra analysis showed that the studied hemicelluloses (TMP and SP) mainly contain mannose, glucose and galactose thus can be described as galactoglucomannan (GGM). HSQC showed no resonances in the aromatic region characteristic of lignin and these samples could be considered as fairly pure in terms of lignin contamination, which is also consistent with the UV spectroscopy analyses. However, a fair amount of arabino glucuronoxylan is also part of the SP sample as previously reported for a similar preparation by Palm and Zacchi.[33] Sample TMP also contains arabino glucuronoxylan but in much lower amount. Traces of 4-O-methylglucoronic acid (4-O-Me-GlcA) were present in the SP sample, which was also reported by Palm and Zacchi.[33]

The 1D proton spectra of both samples at 70 °C is shown in Fig. 2 and corresponds to the general assignments in the anomeric region from Table 3. Apart from the anomeric signals assigned in the fingerprint region (4.4–5.5 ppm), signals at 2.1–2.24 ppm indicate presence of acetylated saccharides. This was further confirmed in HSQC, where typical cross peak for acetyl group is clearly seen in the insert of Fig. 1 at δ_H/δ_C 2.2–1.9/21.56–21.4. Of these acetylated saccharides, HSQC shows that they correspond to β-(1–4)-linked mannopyranosyl

Table 2 Structural properties of different mannans. The GGM chemical analysis is from present work and the reference is for the method of preparation. The guar gum and locust bean gum data is from supplier[38]

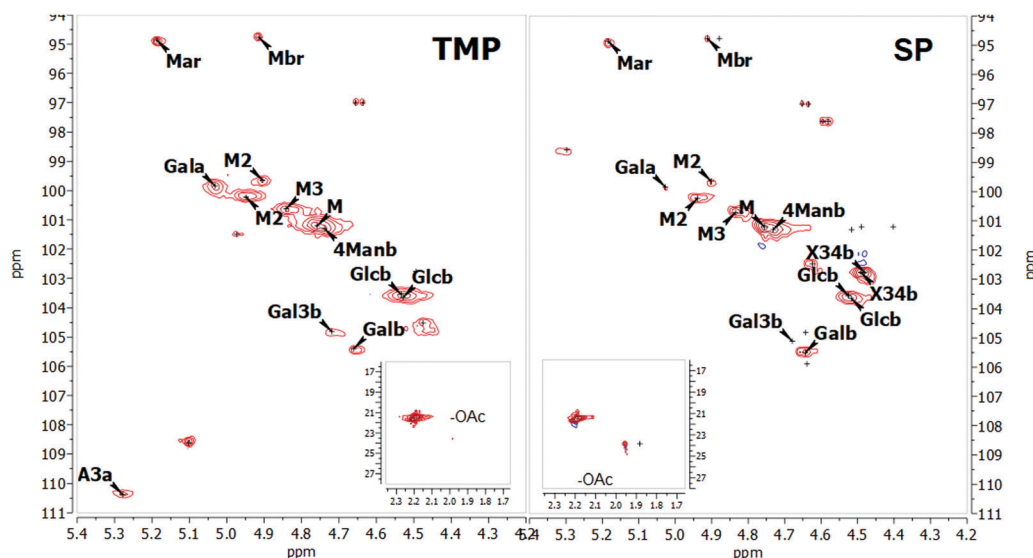| Sample		Molecular weight [kDa]	Molar ratio						Ref.
			Man	Gal	Glc	Acetyl	Ara	Xyl	
Guar gum (GG)		250.0	67	33					38
Locust bean gum	LBG	556.0	78	22					
	LvLBG	107.0	78	22					
Spruce galactoglucomannan	TMP	14.0	50	15	15	20			2, 6 and 33
(GGM)	SP	5.9	40	6	16	2	2	8	

Fig. 1 2D NMR spectra of the anomeric region for the TMP (on the left) and SP (on the right) samples at 25 °C.

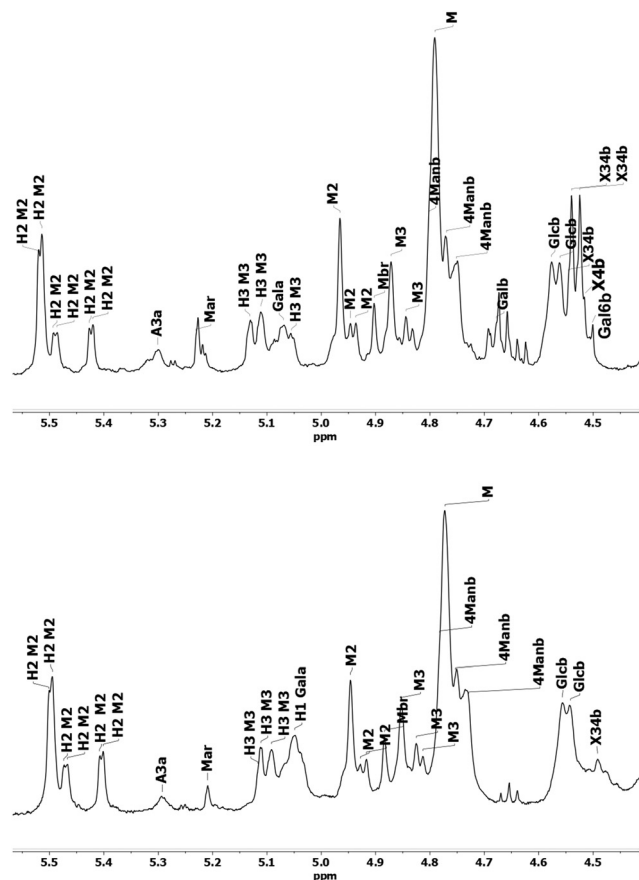This journal is © The Royal Society of Chemistry 2020

Fig. 2 Anomeric region of ^{1}H NMR spectra of O-acetyl-GGM SP (top) and TMP (bottom). Table 3 describes assignations.

Table 3 ^{1}H and ^{13}C NMR data of the anomeric region for the SP-GGM

Constituent	Annotation	Fig. key	^{1}H (ppm)	^{13}C (ppm)
Mannose	α-ManpR	Mar	5.18	94.87
	-4)-β-Manp-(1-, 2-O-Ac	M2	4.94	100.23
	-4)-β-Manp-(1-, 2-O-Ac	M2	4.9	99.65
	β-ManpR	Mbr	4.88, 4.91	94.77
	-4)-β-Manp-(1-, 3-O-Ac	M3	4.83	100.72
	β-Manp-(1-	M	4.76	101.21
	-4)-β-Manp-(1-	4Manb	4.73	101.3
Glucose	-4)-β-Glcp-(1-	Glcb	4.53	103.55
	-4)-β-Glcp-(1-	Glcb	4.52	103.65
Galactose	αGalp-(1-	Gala	5.03	99.84
Other polysaccharides Arabino-xylan	-4,3)-β-Xylp-(1-	X34b	4.48, 4.49	102.77
	α-Araf-(1-3	A3a	5.28^a	
β-Galactan	-4)-β-Galp-(1-	Galb	4.64	105.5
Arabino-galactan	-3)-β-Galp-(1-	Gal3b	4.68	105.11

^{a} From ^{1}H NMR.

residues at C-2 and C-3 as previously reported.[19,59,61] For both acetylated saccharides HSQC showed multiple cross peaks as well as several resonances in the 1D proton spectra (compare with inserts in Fig. 1). This reflects the random distribution of the acetylated residues along the backbone and was also observed by Lundqvist et al.[18]

Ratios of the different sugars were estimated using a semi-quantitative approach based on the volume integration[60,62] from HSQC as well as integration from 1D ^{1}H. The limitation of using volume integrals from HSQC is that the phase in the directly detected dimension varies between the different cross-peaks, with different amounts of the dispersive component contributing, thereby affecting their integral. The disadvantage of using ^{1}H is that with the overlap of peaks the accuracy of the integration is no more than 95% in some cases, this error would propagate when calculating ratios as they involve more than two integrals. Nevertheless, these methods are established and have been extensively used previously.[35,59] Quantification of molar fraction an estimation of masses was also calculated as done in Rosengren et al.,[36] using and external standard and using ERETIC 2 method as described previously. Given that the results from all the methods are comparable here we present the results from the ERETIC 2 based calculations in Tables 4 and 5. We have made the utmost effort to describe the correct assignation of all peaks.

Table 4 shows a summary of the composition estimates for both samples using NMR. The Man : Glu : Gal was estimated to be 100 : 22 : 9 and 100 : 18 : 5 for TMP and SP, respectively. Both samples are fairly similar except in the galactose molar content. Here it should be noted that galactose content is calculated based on α-galactose, the presence of galactan would up this number. GGM in softwood is described usually as substituted with only αGalp units.[19] Furthermore, the galactose peak is not well-resolved (cf. Fig. 2) and the integration is likely to substantial error. We also note that the chemical analysis (Table 2) gives a larger galactose content. The degree of acetylation (DSAc) was estimated by comparing the integrals of the acetylated regions and the GGM sugars in the anomeric region.[60]

Table 4 Total sugar composition of GGM samples

% mol	Man	Glc	αGal	AraXyl	Acetyl	DSAc^a
TMP	64	14	6	5	12	0.15
SP	61	11	3	15	11	0.15

Man – mannose, Gal – galactose, Glc – glucose, AraXyl – arabino xylan. ^{a} The degree of acetylation was determined as the molar ratio of –OAc groups linked to the GGM sugars.

Table 5 Sugar composition of GGM samples in relation to mannose content

% mol	Man	αGal-Man^a	OAc-Man	2-OAc Man	3-OAc Man
TMP	59	1	40	57	43
SP	59	5	36	58	42

Man – (unsubstituted) mannose, Gal – galactose, OAc-Man = 2-OAc + 3-OAc. ^{a} Molar fraction of non-acetylated mannose with galactose substituents assuming that mannose is either substituted with an –OAc or an αGal.

Table 4 shows that the main difference between both samples is the presence of higher amounts of arabino glucurunoxylan constituents in the SP sample (see Table S2, detailed SP NMR peak assignments are shown in ESI†). The given values include the two major residues of arabino glucuronxylan-3,4)-β-Xylp-(1- and α-Araf-(1–3 because they are the major constituents identified unequivocally from the spectra. Other components related to other polysaccharides such as arabinogalactan were not possible to use for quantification given their small area, ambiguity in peak assignation and/or overlapping with other peaks. Based on the values given in Table 4, the ratio of Man : AraXyl of ∼1 : 0.24 was calculated for SP compared to 1 : 0.07 in TMP. Arabino glucuronoxylan is also a hemicellulose common in spent sulfite liquor (SSL) from spruce.[62] It has been shown that small amounts of arabinose and xylose can be covalent constituents of GGM.[63] Nevertheless, the presence of these polysaccharides may be due to hemicellulose contaminants. Other cross peaks related to arabino glucuronoxylan could be assigned to β-Xylp (4.13, 3.38/64.04) as well as the residue 3,4-Xylp in sample SP. Characteristic peaks of α-glucuronic acid were also detected. The cross peaks at 3.47/61.02 and 3.3/73.8 ppm indicate that a fraction of these residues carry the 4-O-methyl substituent.[19]

Table 5 shows the sugar composition in relation to the mannose content. The degree of acetylation (DSAc) was 0.15 in relation to the Manp units for both of the samples. As discussed above, the NMR spectra suggest that the acetylated residues are randomly distributed along the backbone. It is interesting to note that the molar fraction of non-acetylated mannose with galactose substituents is higher for the SP sample, however this can be related to the difficulties in determining the galactose content with NMR.

Dynamic and static light scattering (DLS and SLS). The combination of static and dynamic light scattering gives a measure of the overall shape and size of particles, molecules or aggregates in solution. The ratio between R_G and R_H indicates whether a polymer behaves as a random coil, forms a spherical particle ($R_G/R_H > 0.778$) or has a long rod-like conformation ($R_G/R_H > 2.0$) in solution.[64] Table 6 shows the average R_G and R_H of LBG, GG, LvLBG, TMP and SP GGM. All samples were filtered with 0.45 μm-pore filter to remove larger aggregates and dust that have disproportionally large impact on the scattering data due to their higher scattering power. The correlation functions are listed in the ESI† (Fig. S2).

The molecular weight and dimensions of the GGM monomer estimated from individual sugar groups are 0.18 kDa and 0.6 nm,

respectively. Therefore, fully stretched linear polymer in a monodisperse sample with molecular weights of 14.0 kDa and 5.9 kDa, would be 47 nm and 20 nm long, respectively, which is almost three times lower than the obtained values. Thus, the GGM samples are likely to be aggregated. This conclusion is consistent with cryo-TEM images of TMP GGM at the same concentration (Fig. S4, in the ESI†) and with a recent study of a comparable GGM preparation that shows similar aggregated structures but larger in size,[65] likely due to a higher molecular weight and solution concentration of the sample. The expected contour length of the locust bean gum and guar gum samples, calculated based on the molecular weight of the corresponding linear polymer, is about 10 times larger than the measured value. This suggests that these polysaccharides are not aggregated but form separate polymer chains in solution. Furthermore, both GGMs have a R_G/R_H slightly higher than 1 (Table 6) which suggests that the aggregates have an elongated shape. With a R_G/R_H of around 0.7, LBG and GG chains seems to adopt a globular shape in solution. The radius of gyration for the GG and LBG are similar to literature values.[66,67]

Small-angle X-ray scattering. Fig. 3 shows the scattering curves obtained with SAXS for TMP and SP GGM samples with different molecular weights, as well as branching degree. Samples were characterized at three concentrations 5 mg mL^{-1}, 10 mg mL^{-1} and 20 mg mL^{-1} (Fig. S3, in the ESI†) but no significant difference in scattering was observed for either sample when taking into account the polymer concentration. Therefore, we show only the scattering curves recorded at 10 mg mL^{-1} for each sample. This study is focused on GGM and the galactomannans are to be considered as important reference samples. A detailed SAXS analyses for this type of samples require
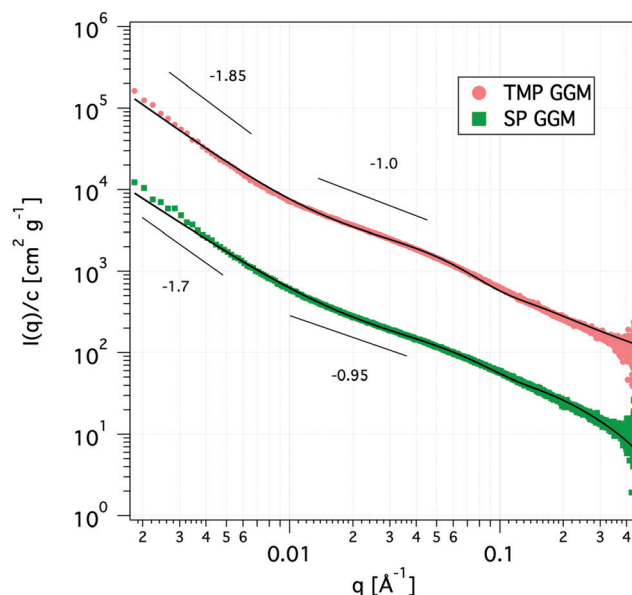

Fig. 3 SAXS curves of the TMP (light red) and SP GGM (green) at a concentration of 10 mg mL^{-1}. Solid lines are fits to the corrected Beaucage model. The scattering curve of the TMP was shifted upwards by a factor of 10 for clarity.

Table 6   Molecular weight and the results obtained from DLS and SLS of the mannan-based polysaccharides

		M_w [kDa]	R_G [nm]	R_H [nm]	R_G/R_H
GGM	TMP	14.0	122	111 ± 8	1.10
	SP	5.9	87	82 ± 6	1.07
Locust bean gum	LvLBG	107.0	79	95 ± 14	0.75
	LBG	556.0	111	210 ± 39	0.53
Guar gum	GG	250.0	42	93 ± 16	0.61

synchrotron X-rays, and unfortunately, we only got limited beam time that was enough to fully characterize the GGM samples.

The scattering curves show no distinct features other than a shift of the power-law decay from −1.85 at low q to −1.0 at high q for TMP GGM (−1.7 to −0.95 for SP GGM) as indicated in Fig. 3. The lack of a drastic change in the slope through the extended q-range indicates self-similarity or fractal-like behaviour of the polymer molecules in solution. The scattering from such a polymer chain can be described by using a mass fractal model, *i.e.* the scattering intensity, $I(q) \sim q^{-d}$. Such a model is valid as the exponents ($-d$) are between −1 and −3.[45] The exponent of −1 at high q-values indicates rod-like shape of the polymer below its persistence length. Based on these observations, the scattering data was fitted to a corrected Beaucage model that describes fractal morphology with flexible cylinders as building blocks.[45,46] This model gives two radii of gyration that were determined from the low-q region and the transition region between two slopes of the scattering curve indicated in Fig. 3. The slope at low-q, *i.e.* in the regime where the Guiner model is valid, R_G represents the overall size of the polymer particle. However, in the case of (large) polymers, it can be challenging to reach the Guinier regime due to limited q-range of most instruments. The second R_G, however, can be converted to a Kuhn length l by using the eqn (6)[68,69]

$$l = \sqrt{12R_G^2} \tag{6}$$

The Kuhn length is twice the persistence length and a measure of the polymer chain stiffness. For the data shown in Fig. 3, we obtained $l = 8.4$ and $l = 11.2$ nm for SP and TMP GGM, respectively. This demonstrates a decreased chain flexibility due to branching, as TMP GGM has a higher galactose substitution degree than SP GGM according to the chemical analysis results (Table 2). This is not shown by NMR though, but here as discussed above the quantification of galactose is a bit uncertain. Another factor that can affect the results is the presence of higher amounts of arabino glucurunoxylan constituents in the SP sample.

Due to a high density of short galactose branches on the polysaccharide backbone, we expect the GGMs to behave as comb-like polymers. A computational study showed that branching considerably stiffens the backbone of comb-like polymers and the Kuhn segment length increases with increasing side chain length due to excluded volume interactions between side chains.[70]

AFM of cellulose film. The microcrystalline cellulose Avicel used in this study for the film formation has a crystalline structure characteristic to a native cellulose I. In order to solubilize cellulose, the strong inter and intramolecular hydrogen bonds need to be broken. This is achieved in LiCl/DMAc solvent as Li⁻ anions form even stronger hydrogen bonds with the hydroxyl group protons of cellulose.[71] By breaking the hydrogen bonding network, cellulose fibres disintegrate into individual polymer chains or smaller bundles that can be dispersed in solution. Thus, it is likely to expect a change of cellulose crystal structure, when the cellulose is recrystallized at

surface from the LiCl/DMAc solvent. In fact after dissolution, the crystallinity index usually decreases to a value typical for a semicrystalline matrix (cellulose III).[72] Different aspects of crystallinity of cellulose and quantification has been thoroughly discussed by Krässig.[73] Important also to consider is the size of the crystalline domains, which can be estimated from broadening of the X-ray powder pattern.[74] Aulin *et al.* has used small incidence angle X-ray diffraction to estimate the crystallinity of thin films of cellulose prepared using different methods and sources.[75] They estimated the crystallinity of the type of surface films used in the present study to be about 15% or less.

Films from dissolved cellulose were characterized with AFM in non-contact mode in air before the ellipsometry and neutron reflectometry experiments. Fig. 4 shows the topographical features of the spin-coated cellulose surface. The surface is uniformly covered with cellulose fibrils associated in random network giving a fairly smooth layer and the root mean square roughness of the film is 3 nm.

We note that the applied protocol gives high reproducibility when it comes to surface structures as observed with AFM in air. Unfortunately, it is not possible to determine the crystallinity of the film with AFM. It was also not possible to image the surfaces under water with the used AFM set-up. This is partly due to swelling of the surface layer as observed by ellipsometry and described further below. Swelling of the cellulose film in water has also been observed by Aulin *et al.*[75]

Ellipsometry. The adsorption of mannans at low concentration (0.02 mg mL^{-1}) were studied *in situ* with null ellipsometry.
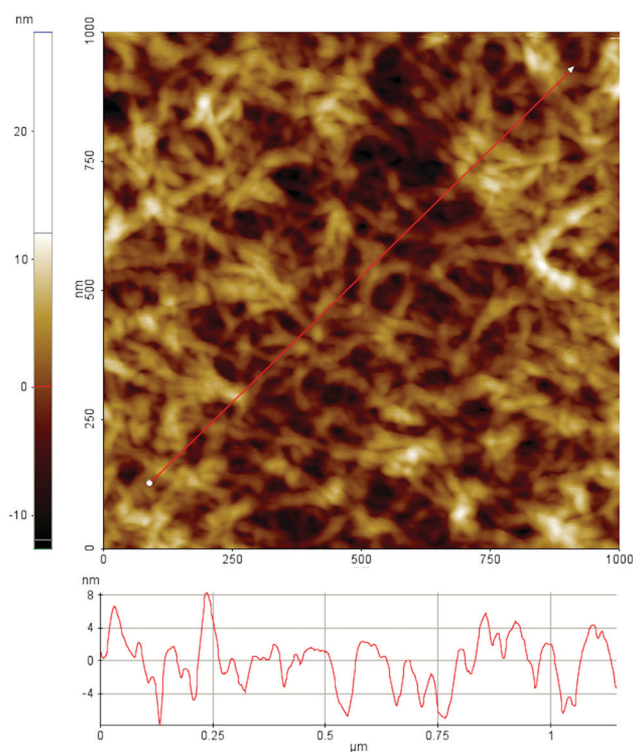

Fig. 4 AFM topography image of a cellulose film spin coated on silica substrate.
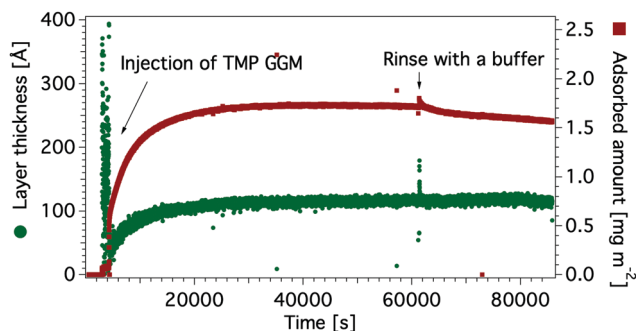
Fig. 5 Adsorbed amount (red) and layer thickness (green) of TMP GGM on a hydrophobic silicon oxide surface.

Fig. 5 shows the results from a typical adsorption measurement. The sample was added to the cuvette after the substrate had been equilibrated in the buffer. The kinetics of the adsorbed amount was then followed and after the plateau in adsorption is reached, the cuvette was rinsed with a neat buffer solution to reveal the reversibility of the adsorption.

Fig. 6 summarizes ellipsometry results for mannans on hydrophobic and cellulose coated surfaces. The adsorption *versus* time data are shown in Fig. S6 and S7, in the ESI.† The adsorbed amount is higher on cellulose surfaces than on hydrophobic surfaces for all studied polysaccharides. This suggests a stronger attractive interaction of mannans to the cellulose surface. One might speculate that this is due to a specific interaction between the two types of polysaccharides, *i.e.* mannans and cellulose. It is known that simple sugar surfactants, *i.e.* hexadecyl maltosides, show strongly attractive head group interactions, which is different for different stereo-isomers and have large effect on the assembly behaviour.[76]

Similar tendency has also been observed with bacterial cellulose produced in the presence of mannan-based polysaccharides leading to a *co*-crystallisation of polysaccharides.[26,32,77] A contributing factor could also be that the rougher cellulose substrate gives a larger effective area and hence a larger number of adsorption sites.

We note that the ellipsometry data has been analysed with a model comprised of individual homogenous layers, *i.e.* silicon, silicon oxide and a top layer consisting of cellulose that also

Fig. 6 Adsorbed amounts of mannan-based polysaccharides on hydrophobic and cellulose surfaces studied by ellipsometry. Data is represented in the order of decreasing polysaccharide molecular weight. Measurements were repeated at least once.

includes mannans after adsorption. We have used an alternative model with a separate mannan layer on top of the cellulose layer (Table S3, ESI†). We would like to remind that the cellulose films prepared with the above described method is expected to have a semicrystalline structure. We also note from the AFM image in Fig. 4 that the film has a rather open structure and we can expect that such a structure can entrap a significant amount of water, leading to swelling of the film. This was also observed with ellipsometry (Fig. S5, in the ESI†). Since the mannan–cellulose surface interaction is more favourable than the water–cellulose surface interaction, mannan polymers adsorb on surface replacing the water molecules.[23] Under such conditions we can regard the adsorption process as entropically driven. Compared to a flat and smooth hydrophobic surface the rougher cellulose surface has also a larger effective area to which hemicellulose can bind.

The adsorbed amount of the mannans to the cellulose surface is dependent on the molecular weight of polymer chains as the highest value was obtained with the 556 kDa Locust bean gum (3.4 ± 0.2 mg m^{-2}) and the lowest one with the 5.9 kDa SP (2.1 ± 0.3 mg m^{-2}) and 14 kDa TMP GGM (2.1 ± 0.1 mg m^{-2}). The effect of the molecular weight on the adsorption of polysaccharides was previously noted by Kabel *et al.*[25] who compared the adsorption of xylans with different molecular weights to bacterial cellulose. However, a study by Hannuksela *et al.*[5] on the interaction between enzymatically modified guar gum and bleached kraft pulp found that the galactose substitution degree has a stronger impact on the adsorbed amount to cellulose than molecular weight. The highest adsorption was found for mannans with lower density of galactose units for both high and low molecular weight samples. The authors suggested that a close contact between mannan backbone and cellulose surface is necessary to obtain high adsorbed amount and a large density of side groups prevents this close contact.

We can conclude that all studied mannan polymers have fairly hydrophobic character based on the ellipsometry results that show significant adsorption on the hydrophobic surface. GGMs give higher adsorbed amount on hydrophobic surfaces than galactomannans. A plausible explanation is the acetylation carried by the GGM backbone but not by the galactomannans (Table 2).

The NMR spectra indicated that the acetylation is randomly distributed along the polysaccharide chain. An additional contributing factor may be the amphiphilic character of sugar monomers, displaying a hydrophobic surface that makes hydrophobic interactions favourable[78] as described *e.g.* for cellulose.[79,80] The hydrophobicity of mannoses is suggested to be similar or even slightly higher than for glucose.[78] With the lower degree of galactosylation of the used GGM (Table 2) it could be argued that the GGM on average have longer unsubstituted backbone regions which potentially, in addition to acetyls, could be responsible for interactions with the hydrophobic surface. All the polysaccharides have higher adsorbed amount on the cellulose surface than on the hydrophobic surface. This is possibly due to attractive interaction between
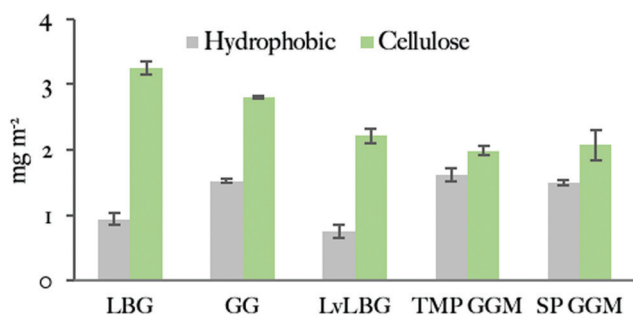
Table 7 The summary of the adsorbed amounts on hydrophobic surfaces as followed with ellipsometry and QCM-D, and the calculated solvent content in the adsorbed layer

		LBG	GG	LvLBG	TMP GGM	SP GGM
Adsorbed amount (mg m^{-2})	QCM-D	26 ± 6	30 ± 10	31 ± 4	28 ± 3	28 ± 1
	Ellipsometry	0.94 ± 0.09	1.53 ± 0.03	0.8 ± 0.1	1.6 ± 0.1	1.50 ± 0.03
Solvent content [%]		96	95	97	94	95

the carbohydrate groups of the adsorbing polymer and those in the cellulose surface. Although this cannot be the driving force of the hemicellulose attachment, it can possibly make the adsorption less reversible. In this respect, it can lead to an apparently higher adsorption. In addition, the more open structure of the cellulose film will lead to higher specific area as discussed above. The adsorption was found to increase with the molecular weight and in contrast to the study of Hannuksela *et al.*,[5] we did not find a correlation between difference in branching as indicated by the chemical analysis (Table 2) and adsorption.

Quartz crystal microbalance with dissipation. The adsorption of mannan-based polysaccharides on hydrophobic surface was studied using QCM-D. The adsorbed amount on hydrophobic surfaces was obtained from fitting the data to the Voigt viscoelastic model, see ESI† (Fig. S8, in the ESI†). The adsorbed amounts recorded by QCM-D (Table 7) are significantly higher than those obtained with ellipsometry. This is because QCM-D measures the wet mass of the adsorbed layer that includes coupled water. The combined results from ellipsometry and QCM-D show that the adsorbed mannan layer is highly hydrated with the solvent amount above 90%. Here is noteworthy that the SAXS data suggest that the GGM polymer chains are quite stiff, presumably due to the presence of galactose side chains. Unless the GGM chain is parallel to the surface, portions of the GGM molecules will extend into solution and contribute to the large added amount as revealed with QCM-D, *i.e.* larger amount of coupled water. The high content of water in the adsorbed layers of mannans have already been reported previously with 91% for GG and 65% for GGM.[28,81] However, the dry mass of the added layer of GG and GGM on cellulose (0.26 mg m^{-2} and 0.6 mg m^{-2}) is much lower than the one obtained in the current study (2.8 mg m^{-2} and 2.0 mg m^{-2}) with the ellipsometry. This could be explained by the difference in the thickness of the cellulose layer. As shown in Fig. S9 (in the ESI†), the thickness of a cellulose layer has a significant effect on the adsorbed amount of the mannan.

Neutron reflectometry. Neither ellipsometry nor QCM-D allows for a determination of the density profile of the adsorbed biopolymer layer perpendicular to the surface; the adsorption of TMP GGM on hydrophobic surface was therefore studied with neutron reflectometry. The reflectivity curves and modelling results are shown in Fig. 7. The model fit parameters are summarized in Table 8.

A significant change in the measured reflectivity is observed after the addition of TMP GGM compared to the bare surface, although the changes in the measurements with H$_2$O solvent
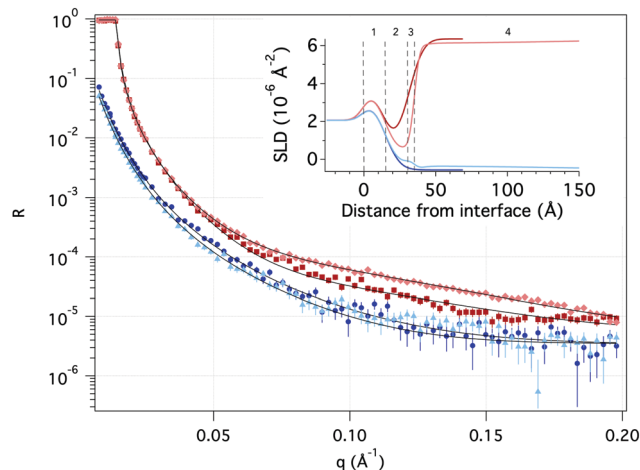

Fig. 7 Neutron reflectivity as a function of momentum transfer (*q*) of pure hydrophobic surface (dark red in D$_2$O and dark blue in H$_2$O) and after adsorption of TMP (light red in D$_2$O and light blue in H$_2$O). Solid black lines represent the theoretical fit. The inset illustrates the scattering length density (SLD) profile as a function of distance from the Si surface based on the fitting with the numbers indicating layers described in Table 8.

are smaller due to the comparatively low scattering contrast between H$_2$O and TMP GGM.

The best fit to the data with a χ^2 of 3.6 was obtained by using a simple optical model where the TMP GGM layer is divided into two. Here, the layer closest to the hydrophobic surface is expected to have more of GGM moieties with acetyl groups and parts of the hydrophobic layer *i.e.* the transition layer. The top layer is expected to be much more hydrated with more of the non-acetylated sugar moieties. The roughness takes care of the fact there are no sharp borders between the layers, but rather a (Gaussian) distribution of matter.

The transition layer is around 4 Å with the scattering length density (SLD) equal to 0.7×10^{-6} Å^{-2} in D$_2$O and 0.5×10^{-6} Å^{-2} in H$_2$O. This suggests that there is very little water in this layer. The top layer is 210 Å with the SLD of 3.4×10^{-6} Å^{-2} and 1.9×10^{-6} Å^{-2} in D$_2$O and H$_2$O, respectively. According to Raghuwanshi *et al.*[82] every glucose unit in cellulose contains three hydrogens that are instantly exchanged with deuterium, therefore SLD of the polysaccharide is different in D$_2$O and H$_2$O. The top layer is much thinner than expected from the hydrodynamic radius (see Table 6), indicating that the polymer takes a flat conformation on the hydrophobic surface. As we have shown previously by combining the results obtained with ellipsometry and QCM-D, the top layer is highly hydrated with the solvent amount of 97%.

Table 8 Parameters obtained from the fitting of NR data measured in D_2O and H_2O. The numbers correlate to the layer numbers in the SLD profile in Fig. 7

	1	2	3		4	
	SiO_x	Hydrophobic layer	Transition layer		GGM	
			D_2O	H_2O	D_2O	H_2O
SLD [10^{-6} Å^{-2}]	3.47	-0.44 ± 0.02	0.68 ± 0.08	0.5 ± 0.4	3.4 ± 0.1	1.9 ± 0.5
Layer thickness [Å]	15.6 ± 0.2	15.8 ± 0.1	4.0 ± 0.2		210 ± 11	
Solvent [v/v, %]	8.7 ± 0.6	6.9 ± 0.3	14 ± 1		97.1 ± 0.1	
Roughness [Å]	8.2 ± 0.1	8.3 ± 0.1	2.1 ± 0.2		97 ± 13	

Conclusions

The nature of the interactions between hemicellulose and cellulose is important for both understanding the processes inside plant cell walls, as well as a tool for development of various sustainable materials to replace fossil-based ones. Although these interactions have been studied since 1980s, the nature of the interactions are still not fully understood due to lack of access to well-defined samples and challenges when it comes to preparation of samples and characterisation techniques.

The main aim of this work was to reveal the structural properties of softwood hemicellulose that controls their affinity to cellulose surfaces. The adsorption of softwood hemicellulose (GGM) and similar galactomannans was studied with ellipsometry, QCM-D and neutron reflectometry. To provide further understanding of the forces that control the interaction between hemicellulose and cellulose, the adsorption was also performed on the hydrophobised silica. The combined results from these measurements show:

1. All polymers showed a higher adsorbed amount on the cellulose surface than on the hydrophobic one. This can be related to the larger specific area of the cellulose layer. In addition, attractive interaction between the adsorbing polymer sugar groups and corresponding groups in the cellulose layer might contribute to anchoring the polymer to the surface.

2. The substantial adsorption to the hydrophobic surface indicates that the polysaccharides have a fairly hydrophobic character. The results also suggest that GGM samples are more hydrophobic as shown by NR possibly due to the presence of acetyl side groups in the GGM structure that interact with the hydrophobic surface.

Cellulose films prepared in this study are expected to have a semi-crystalline nature with amorphous regions entrapping large amount of water molecules. The interaction between mannan and cellulose molecules are more favourable than cellulose–water interaction due to relatively hydrophobic nature of both polymers. We therefore expect that increase of entropy due to the release of water upon adsorption is one of the driving forces.

Mannans form a diffuse monolayer with parts extending into the solution as observed by QCM-D and NR. This is supported by the SAXS data showing that GGMs are quite stiff, likely due to bulky galactose side groups. DLS, SLS and Cryo-TEM indicate that polymers are present in the solution in the aggregated state. However, the observed thickness of the layer is smaller, which indicates that they rearrange and take flat conformation at the interface.

The adsorption to cellulose coated surface increases with the molecular weight, however, no clear impact of the galactose substitution degree was found.

Conflicts of interest

There are no conflicts to declare.

Acknowledgements

References

1 E. Sjostrom, *Wood chemistry: fundamentals and applications*, Gulf professional publishing, 1993.

2 J. Lundqvist, A. Jacobs, M. Palm, G. Zacchi, O. Dahlman and H. Stålbrand, *Carbohydr. Polym.*, 2003, **51**, 203–211.

3 H. V. Scheller and P. Ulvskov, *Annu. Rev. Plant Biol.*, 2010, **61**, 263–289.

4 S. Willför, K. Sundberg, M. Tenkanen and B. Holmbom, *Carbohydr. Polym.*, 2008, **72**, 197–210.

5 T. Hannuksela, M. Tenkanen and B. Holmbom, *Cellulose*, 2002, **9**, 251–261.

6 A. Andersson, T. Persson, G. Zacchi, H. Stålbrand and A.-S. Jönsson, *Appl. Biochem. Biotechnol.*, 2007, **137**, 971–983.

7 B. Al-Rudainy, M. Galbe and O. Wallberg, *Sep. Purif. Technol.*, 2017, **187**, 380–388.

8 B. Al-Rudainy, M. Galbe, H. Schagerlöf and O. Wallberg, *Holzforschung*, 2018, **72**, 839–850.

9 B. Ünal, S. Metin and N. D. Işikli, *Int. Dairy J.*, 2003, **13**, 909–916.

10 P. K. Soma, P. D. Williams and Y. M. Lo, *Front. Chem. Eng. China*, 2009, **3**, 413–426.

11 M. A. Cerqueira, A. I. Bourbon, A. C. Pinheiro, J. T. Martins, B. W. S. Souza, J. A. Teixeira and A. A. Vicente, *Trends Food Sci. Technol.*, 2011, **22**, 662–671.

12 S. Parija, M. Misra and A. K. Mohanty, *J. Macromol. Sci., Rev. Macromol. Chem. Phys.*, 2001, **41**, 175–197.

13 A. Ebringerová, Z. Hromádková, V. Hříbalová, C. Xu, B. Holmbom, A. Sundberg and S. Willför, *Int. J. Biol. Macromol.*, 2008, **42**, 1–5.

14 K. S. Mikkonen, M. I. Heikkilä, H. Helén, L. Hyvönen and M. Tenkanen, *Carbohydr. Polym.*, 2010, **79**, 1107–1112.

15 J. Hartman, A. C. Albertsson, M. S. Lindblad and J. Sjöberg, *J. Appl. Polym. Sci.*, 2006, **100**, 2985–2991.

16 J. Hartman, A. C. Albertsson and J. Sjöberg, *Biomacromolecules*, 2006, **7**, 1983–1989.

17 A. Doliška, S. Willför, S. Strnad, V. Ribitsch, K. S. Kleinschek, P. Eklund and C. Xu, *Holzforschung*, 2012, **66**, 149–154.

18 J. Lundqvist, A. Teleman, L. Junel, G. Zacchi, O. Dahlman, F. Tjerneld and H. Stålbrand, *Carbohydr. Polym.*, 2002, **48**, 29–39.

19 T. Hannuksela and C. Herve du Penhoat, *Carbohydr. Res.*, 2004, **339**, 301–312.

20 T. Hayashi, K. Ogawa and Y. Mitsuishi, *Plant Cell Physiol.*, 1994, **35**, 1199–1205.

21 Å. Linder, R. Bergman, A. Bodin and P. Gatenholm, *Langmuir*, 2003, **19**, 5072–5077.

22 J.-P. Vincken, A. de Keizer, G. Beldman and A. G. J. Voragen, *Plant Physiol.*, 1995, **108**, 1579–1585.

23 T. Benselfelt, E. D. Cranston, S. Ondaral, E. Johansson, H. Brumer, M. W. Rutland and L. Wågberg, *Biomacromolecules*, 2016, **17**, 2801–2811.

24 T. Hayashi, T. Takeda, K. Ogawa and Y. Mitsuishi, *Plant Cell Physiol.*, 1994, **35**, 893–899.

25 M. A. Kabel, H. van den Borne, J.-P. Vincken, A. G. J. Voragen and H. A. Schols, *Carbohydr. Polym.*, 2007, **69**, 94–105.

26 K. I. Uhlin, R. H. Atalla and N. S. Thompson, *Cellulose*, 1995, **2**, 129–144.

27 S. Ahola, P. Myllytie, M. Osterberg, T. Teerinen and J. Laine, *BioResources*, 2008, **3**, 1315–1328.

28 P. Eronen, K. Junka, J. Laine and M. Österberg, *BioRes*, 2011, **6**, 4200–4217.

29 S. Gao and K. Nishinari, *Biomacromolecules*, 2004, **5**, 175–185.

30 S. Gao and K. Nishinari, *Colloids Surf., B*, 2004, **38**, 241–249.

31 J.-y. Liu, H.-c. Wang, Y. Yin, N. Li, P.-l. Cai and S.-l. Yang, *Carbohydr. Polym.*, 2012, **89**, 158–162.

32 T. Iwata, L. Indrarti and J. I. Azuma, *Cellulose*, 1998, **5**, 215–228.

33 M. Palm and G. Zacchi, *Sep. Purif. Technol.*, 2004, **36**, 191–201.

34 F. Örså, B. Holmbom and J. Thornton, *Wood Sci. Technol.*, 1997, **31**, 279–290.

35 R. Schröder, P. Nicolas, S. J. Vincent, M. Fischer, S. Reymond and R. J. Redgwell, *Carbohydr. Res.*, 2001, **331**, 291–306.

36 A. Rosengren, S. J. Butler, M. Arcos-Hernandez, K.-E. Bergquist, P. Jannasch and H. Stålbrand, *Green Chem.*, 2019, **21**, 2104–2118.

37 G. Wider and L. Dreier, *J. Am. Chem. Soc.*, 2006, **128**, 2571–2576.

38 Megazyme, https://www.megazyme.com, accessed December 2017.

39 R. Sczech and H. Riegler, *J. Colloid Interface Sci.*, 2006, **301**, 376–385.

40 D. P. Chang, M. Jankunec, J. Barauskas, F. Tiberg and T. Nylander, *ACS Appl. Mater. Interfaces*, 2012, **4**, 2643–2651.

41 T. Zemb and P. Lindner, *Neutron, X-Rays and Light. Scattering Methods Applied to Soft Condensed Matter*, North Holland, 2002.

42 D. E. Koppel, *J. Chem. Phys.*, 1972, **57**, 4814–4820.

43 SasView, https://www.sasview.org/, accessed February 2019.

44 G. Beaucage, *J. Appl. Crystallogr.*, 1995, **28**, 717–728.

45 B. Hammouda, *J. Appl. Crystallogr.*, 2010, **43**(6), 1474–1478.

46 G. Beaucage, *J. Appl. Crystallogr.*, 1996, **29**, 134–146.

47 F. Tiberg and M. Landgren, *Langmuir*, 1993, **9**, 927–932.

48 J. A. De Feijter, J. Benjamins and F. A. Veer, *Biopolymers*, 1978, **17**, 1759–1772.

49 G. Robinson, S. B. Ross-Murphy and E. R. Morris, *Carbohydr. Res.*, 1982, **107**, 17–32.

50 C. Xu, A. Pranovich, L. Vähäsalo, J. Hemming, B. Holmbom, H. A. Schols and S. Willför, *J. Agric. Food Chem.*, 2008, **56**, 2429–2435.

51 Y. Ono, T. Ishida, H. Soeta, T. Saito and A. Isogai, *Biomacromolecules*, 2016, **17**, 192–199.

52 M. V. Voinova, M. Jonson and B. Kasemo, *Spectroscopy*, 2004, **18**(4), 537–544.

53 M. V. Voinova, M. Rodahl, M. Jonson and B. Kasemo, *Phys. Scr.*, 1999, **59**, 391.

54 J. Penfold and R. Thomas, *J. Phys.: Condens. Matter*, 1990, **2**, 1369–1412.

55 J. A. Dura, D. J. Pierce, C. F. Majkrzak, N. C. Maliszewskyj, D. J. McGillivray, M. Lösche, K. V. O'Donovan, M. Mihailescu, U. Perez-Salas, D. L. Worcester and S. H. White, *Rev. Sci. Instrum.*, 2006, **77**(7), 74301–7430111.

56 B. Maranville, W. Ratcliff II and P. Kienzle, *J. Appl. Crystallogr.*, 2018, **51**, 1500–1506.

57 A. Nelson, *J. Appl. Crystallogr.*, 2006, **39**, 273–276.

58 A. Nelson, *J. Phys.: Conf. Ser.*, 2010, **251**, 012094.

59 B. Al-Rudainy, M. Galbe, M. Arcos Hernandez, P. Jannasch and O. Wallberg, *Polymers*, 2019, **11**, 35.

60 J. Berglund, S. Achar, M. Lawoko, M. Lindström, F. Vilaplana, J. Wohlert and G. Henriksson, *Cellulose*, 2019, **26**, 2155–2175.

61 H. Lindqvist, J. Holmback, A. Rosling, K. Salminen, B. Holmbom, M. Auer and A. Sundberg, *BioResources*, 2013, **8**, 994–1010.

62 B. Al-Rudainy, M. Galbe, F. Lipnizki and O. Wallberg, *Membranes*, 2019, **9**, 99.

63 I. M. Sims, D. J. Craik and A. Bacic, *Carbohydr. Res.*, 1997, **303**, 79–92.

64 W. Burchard, *Laser light scattering in biochemistry*, 1992, pp. 3–22.

65 S. Kishani, F. Vilaplana, W. Xu, C. Xu and L. Wågberg, *Biomacromolecules*, 2018, **19**, 1245–1255.

66 D. R. Picout, S. B. Ross-Murphy, N. Errington and S. E. Harding, *Biomacromolecules*, 2001, **2**, 1301–1309.

67 D. R. Picout, S. B. Ross-Murphy, K. Jumel and S. E. Harding, *Biomacromolecules*, 2002, **3**, 761–767.

68 B. W. Mansel, C.-Y. Chu, A. Leis, Y. Hemar, H.-L. Chen, L. Lundin and M. A. K. Williams, *Biomacromolecules*, 2015, **16**, 3209–3216.

69 P. Hernandez-Cerdan, B. Mansel, A. Leis, L. Lundin and M. A. K. Williams, *On the Structural Analysis of Polysaccharide-Networks by Transmission Electron-Microscopy: Comparison with SAXS*, 2018.

70 Y. Nakamura and T. Norisuye, *Polym. J.*, 2001, **33**, 874–878.

71 C. Zhang, R. Liu, J. Xiang, H. Kang, Z. Liu and Y. Huang, *J. Phys. Chem. B*, 2014, **118**, 9507–9514.

72 A. L. Da Róz, F. L. Leite, L. V. Pereiro, P. A. P. Nascente, V. Zucolotto, O. N. Oliveira and A. J. F. Carvalho, *Carbohydr. Polym.*, 2010, **80**, 65–70.

73 H. A. Krässig, *Cellulose, structure, accessibility and reactivity*, Gordon and Breach Publishers, Philadelphia, PA, 1993.

74 C. J. Garvey, I. H. Parker and G. P. Simon, *Macromol. Chem. Phys.*, 2005, **206**, 1568–1575.

75 C. Aulin, S. Ahola, P. Josefsson, T. Nishino, Y. Hirose, M. Österberg and L. Wågberg, *Langmuir*, 2009, **25**, 7675–7685.

76 J. Larsson, A. Sanchez-Fernandez, N. Mahmoudi, L. C. Barnsley, M. Wahlgren, T. Nylander and S. Ulvenlund, *Langmuir*, 2019, **35**(43), 13904–13914.

77 S. E. C. Whitney, J. E. Brigham, A. H. Darke, J. S. G. Reid and M. J. Gidley, *Carbohydr. Res.*, 1998, **307**, 299–309.

78 M. Janado and Y. Yano, *J. Solution Chem.*, 1985, **14**, 891–902.

79 C. Yamane, T. Aoyagi, M. Ago, K. Sato, K. Okajima and T. Takahashi, *Polym. J.*, 2006, **38**, 819–826.

80 B. Lindman, G. Karlström and L. Stigsson, *J. Mol. Liq.*, 2010, **156**, 76–81.

81 P. Eronen, M. Österberg, S. Heikkinen, M. Tenkanen and J. Laine, *Carbohydr. Polym.*, 2011, **86**, 1281–1290.

82 V. S. Raghuwanshi, J. Su, C. J. Garvey, S. A. Holt, W. Raverty, R. F. Tabor, P. J. Holden, M. Gillon, W. Batchelor and G. Garnier, *Cellulose*, 2017, **24**, 11–20.